Hindawi
Adsorption Science & Technology
Volume 2023, Article ID 4319053, 17 pages
https://doi.org/10.1155/2023/4319053

Research Article

Biosorption of Congo Red Dye from Aqueous Solution Using Adsorbent Prepared from *Vangueria infausta* Fruit Pericarp

Aisha Kitemangu, Maheswara Rao Vegi, and Nyemaga Masanje Malima

Department of Chemistry, College of Natural and Mathematical Sciences, University of Dodoma, P.O. Box 259, Dodoma, Tanzania

Correspondence should be addressed to Maheswara Rao Vegi; vegi.rao@udom.ac.tz

Received 5 September 2022; Revised 17 February 2023; Accepted 1 July 2023; Published 29 July 2023

Academic Editor: Lingzhi Yang

The adsorption efficiency of acid-treated *Vangueria infausta* fruit pericarp (VIFP) biosorbent to uptake Congo red (CR) dye was investigated through batch experiments. Optimum conditions for the adsorption process were determined by varying the solution pH, biosorbent dosage, contact time, initial concentration of CR dye, and temperature. Results revealed that the data fits well with the Langmuir isotherm model, demonstrating the monolayer coverage of the CR dye molecule on the surface of the VIFP biosorbent. The higher value of correlation coefficient, R^2 for pseudo-second-order (0.9997) compared to R^2 of pseudo-first-order (0.9605) suggests that the pseudo-second-order kinetic model is an ideal fit in describing the kinetics of CR dye adsorption by VIFP biosorbent. The positive value of ΔH° (41.42 kJ/mol) and ΔS° (158.32 J/mol.K) depicts the endothermic nature and spontaneity of the biosorption of CR dye by VIFP. The values of ΔG° obtained were negative, showing that the adsorption is thermodynamically favourable. Therefore, the acid-treated adsorbent from *Vangueria infausta* can efficiently be used in the removal of CR dye from aqueous solution.

1. Introduction

Globally, water pollution by organic dyes is increasingly becoming a serious environmental issue. Dyes are stable, soluble organic compounds extensively employed in the paper, textile, pharmaceutical, and leather industries [1]. Worldwide, 700,000 tons of dyes and 100 tons of dye waste are produced and discharged into water bodies, respectively [2]. In particular, azo dyes make up 70% of all synthetic dyes used in textile, printing, and paper manufacturing industries [3].

Congo red (CR, $C_{32}H_{22}N_6Na_2O_6S_2$) has two azo groups (-N=N-); thus, it is an excellent model among the synthetic dyes (Figure 1(a)). In a pH range of 5-10, it appears red and has a complex structure with high molecular weight. Owing to its structural complexity and stability, this ionic diazo dye is difficult to biodegrade, accounting for its persistence in the environment. Like other azo dyes, CR metabolizes benzidine, which is carcinogenic and toxic [4]. Although most countries have banned CR dye, it is still employed as a pH indicator, in diagnostic medicine and fields such as microbiology for staining. Extensive use of CR dyes has led to their massive discharge through the soil and wastewater systems. As a result, there is a severe problem with the availability of safe drinking water [5].

Furthermore, suppose the discharged CR dyes are not adequately treated. In that case, they will spend a significant amount of time in the environment, posing a threat to the survival of both terrestrial and aquatic organisms. Therefore, it is of economic and environmental importance to search for effective methods to remove these azo dyes before discharging them into the aquatic environment.

To date, azo dyes have been removed from wastewater using a variety of chemical, biological, and physical approaches [6]. However, although chemical methods can remove dye contaminants swiftly and efficiently, their high costs make them unfavourable for current commercial use. Likewise, besides the simplicity and ecofriendliness of the biological methods, their setup involves bioreactors which demand large space, and their operation proceeds by generating excess sludge [7]. In addition, most azo dyes' structural complexity and stability,

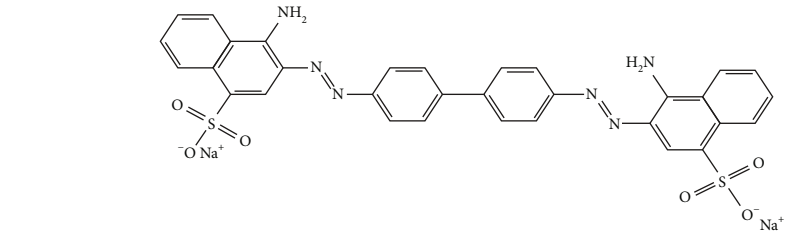

(a)

(b)

(c)

Figure 1: (a) Molecular structure of CR dye. (b) *Vangueria infausta* tree. (c) *Vangueria infausta* fruit.

including CR dye, present high resistance to chemical and biological methods, making their removal from water challenging [8].

Compared to other conventional methods, adsorption is preferred for dye removal due to its inexpensiveness, adsorbent versatility, simplicity, less sludge production, and high efficiency [9]. Various adsorbents such as chitosan, zeolites, clays, polymeric resins, and activated carbon materials have been reportedly employed for dye removal from aqueous solutions. However, their application is constrained by their ineffectiveness at low adsorbate concentration, costly operating process, poor selectivity, and the problem of unsuccessful removal of the colouration from wastewater [10–14]. On the other hand, nanoparticles are emerging as potential adsorbents for water remediation. Still, because of their small size, their separation and recovery from contaminated water pose significant challenges for water treatment. Also, with increasingly widespread applications of nanoparticles in water remediation, there are growing concerns about their potential toxicity to the environment and human health. It is evident from the literature that several nanomaterials may have adverse effects on the environment and human health [15–17].

Similarly, metal-organic frameworks (MOFs) have also attracted colossal research interest in water decontamination. Still, their applications are hampered by their lack of durability and limited availability of raw materials for MOF production [18]. To circumvent these problems, researchers have devoted enormous effort to preparing and using biosorbents because they are readily accessible and can easily be regenerated for further use. Munagapati et al., for example, evaluated the efficacy of modified banana peels to remove reactive black 5 dye from aqueous solutions, achieving a maximum adsorption capacity of 211.8 mg/g [19]. Latif et al. demonstrated the removal of fluorescein and eosin dyes from wastewater by utilizing *Citrullus lanatus*, achieving removal efficiencies of 48.06-88.08% and 48.47-79.31%, respectively [20]. Aminated sunflower seed hulls have also been studied to remove reactive blue 5 and reactive yellow 84 with a maximum uptake of 51.02 mg/g and 63.27 mg/g, respectively [21].

So far, no studies on using *Vangueria infausta* fruit pericarp for the remediation of wastewater contaminated by CR dyes have been reported. *Vangueria infausta* plants grow wildly in most African societies. Trees (Figure 1(b)) bear fruits (Figure 1(c)), which are consumed by humans as well as animals. The extracts from root bark have been reported to exhibit antimalarial activity, while the leaves and stem barks have also been proven to be a remedy for various ailments [22]. The fruit pericarp is a lignocellulosic material constituting natural polymers composed of hemicelluloses, cellulose, lignin, and tannins with hydroxyl groups in each molecule [23–25]. These materials are endowed with functionalities which show promising potential for the adsorption of environmental pollutants, including heavy metals and organic dyes. It is known that the juice industry discards a large amount of waste pericarps and, if left in the environment without proper treatment, would decompose and pollute the environment, eventually threatening public health. Preparing adsorbents from *Vangueria infausta* fruit pericarp (VIFP) is anticipated to solve two ecological problems: pericarp waste recycling and azo dye removal from wastewater. Therefore, this study reports the remediation of Congo red dye using an adsorbent prepared from *Vangueria infausta* fruit pericarp (VIFP).

2. Materials and Methods

2.1. Biosorbent Sampling, Reagents, and Chemicals. The dry *Vangueria infausta* fruits were collected at Issuna village,

located in Ikungi district in Singida region, Tanzania. Reagents and chemicals used in this study were purchased from Thermo Fisher Scientific manufacturer. The reagents and chemicals were of analytical grade and included HCl (35-37%), HNO_3 (69-72%), NaOH (97%), deionized water, and Congo red dye ($C_{32}H_{22}N_6Na_2O_6S_2$). HNO_3 was used to activate the biosorbent while HCl and NaOH were utilized for pH regulation.

2.2. Biosorbent Preparation. The ripe fruits were collected from *Vangueria infausta* trees and dried under a shed for one month. After drying, the fruit pericarps were isolated from the seeds and pulp and rinsed using deionized water. Moisture was removed by oven drying at 353 K to a constant mass. The dried pericarps were then crushed and pulverized into a fine powder and sieved to attain particle sizes ≤ 300 μm. 36 g of the powder was soaked in 500 mL of 0.1 M HNO_3 at 323 K for 24 h to expose the binding sites of the biosorbent. The mixture was then filtered using the Whatman filter paper of 0.45 microns, and the acid content in the residue was removed by washing the powder thoroughly with deionized water. Finally, the filtered biomass was oven dried at 378 K for two hours until a constant mass of 35.160 g was recorded and sealed in air-tight glass bottles to prevent it from moisture [26].

2.3. Physicochemical Characterisation of the Biosorbent. The physical characteristics of the biosorbent, including specific surface area, pore size, and total pore volume, were calculated by the BET method using Quanta Chrome NOVA 1200e surface area and a pore size analyser. All samples were degassed under vacuum at 573 K for six hours and a pressure of 0.1 millitorrs to remove volatiles. Pure liquid nitrogen at 77.35 K was used to determine the specific surface area of the biosorbent through physical adsorption. Surface characteristics were elucidated by JEOL JSM-7500F field emission scanning microscope (FESEM) and transmission electron microscopy (TEM) using a JEOL 1400 TEM, whereby the images were acquired digitally with a Megaview III camera and recorded and measured with the iTEM software of the soft imaging system. Elucidation of biosorbent functional groups before and after acid activation was done using Bruker Optics ALPHA-E FT-IR spectrometer at an absorption range of 4000-400 cm^{-1}. The crystalline structure of the biosorbent was studied by employing a Bruker AXS D8 Advance X-ray diffractometer. The analysis was done under a CuKα monochromatic beam (wavelength of 0.154 nm) produced at 40 KV and 30 mA.

2.4. Preparation of Congo Red (CR) Stock Solution. The adsorbate stock solution with a concentration of 500 mg/L was prepared by dissolving 0.5 g CR in 1 L deionized water. The intermediate solution of 100 mg/L was diluted with deionized water to the required volumes to obtain working solutions.

2.5. Determination of CR Concentration. Quantification of CR was carried out by UV-Vis spectrophotometer (single beam 60 Cary, Agilent Technology UV-Vis) using Chemetrix software. The wavelength that correlated to the maximum absorbance was measured by recording the UV-Vis spectrum using 50 mg/L of CR dye at different pH values of 2, 3, 4, 5, 6, 7, 8, 9, and 10. The pH adjustment was performed using 0.1 M HCl or 0.1 M NaOH. The maximum absorption of 499 nm for pH 5, 6, 7, 8, 9, and 10 and 564 nm for pH 2, 3, and 4 was used for all other measurements. The instrument was calibrated by preparing five standard solutions of CR dye at 5, 10, 15, 20, and 25 mg/L and a reagent blank. The absorbance was measured for each standard as well as the reagent blank. Corrected absorbance was determined by subtracting the reagent blank from the absorbance of other standards. Calibration curves with a correlation coefficient of at least 0.9999 were generated by computer Chemetrix software using the corrected absorbance against the concentration of the standards. These curves were utilized to figure out the unknown concentration of CR dye in the solution [23].

2.6. Batch Adsorption Experiment. The influence of the experimental parameters, including pH, biosorbent dosage, contact time, initial CR dye concentration, and temperature, was carried out to determine the optimum condition for the adsorption of CR dye onto VIFP biosorbent. This was achieved by varying one parameter after another while using the optimum condition obtained from the preceding experiment sequentially.

2.6.1. Effect of pH. The effect of pH on CR adsorption was studied over a pH range of 2-10 by adjusting the pH of the solution using either 0.1 M HCl or NaOH. 50 mL of a solution of CR dye (50 mg/L) was mixed with 0.5 g of VIFP biosorbent in a 250 mL conical flask and stirred at 200 rpm for 180 minutes. The mixture was then filtered, and the remaining CR concentration was analysed from the supernatant by UV-visible spectrophotometer at a wavelength of maximum absorption of 499 nm for pH 5-10 and 564 nm for pH 2-4. To determine the point of zero charge, 1 g of VIFP was placed in 9 flasks of 250 mL, each containing 80 mL of 0.1 M NaCl solution. The pH of the solutions varied from 2 to 10. The mixture was shaken for 24 h at 298 K to 200 rpm in a shaker. The suspension was filtered by the Whatman filter paper of 0.45 microns, and the final pH was recorded.

2.6.2. Effect of Biosorbent Dosage. The effect of biosorbent dosage was studied by equilibrating 50 mL of a solution of CR (50 mg/L) with different masses of biosorbent (0.1, 0.2, 0.3, 0.4, 0.5, 0.6, 0.7, 0.8, and 0.9 g) at the optimum pH and agitated at 200 rpm for 180 min. Then, the mixture was centrifuged, and the supernatant analysis for the remaining dye was done using a UV-Vis spectrophotometer.

2.6.3. Effect of Contact Time. The optimum contact time required for the adsorption of CR was determined using the biosorbent prepared. The optimum VIFP dosage of 0.7 g was contacted with a 50 mL solution of 50 mg/L CR and adjusted to the optimum pH. The solutions were agitated at 200 rpm at different contact times of 30, 60, 90, 120, 150, 180, and 210 min. The mixtures were centrifuged, and the analysis of the supernatant for the remaining dye was done using a UV-visible spectrophotometer.

2.6.4. Effect of Initial CR Dye Concentration. 50 mL of CR dye with different initial concentrations of 10, 20, 30, 40, 50, 60, 70, and 80 mg/L was contacted with 0.7 g of VIFP biosorbent. The mixture was agitated at 200 rpm at a pH of 2 for 180 min. The mixture was centrifuged, and analysis of the supernatant for the remaining dye was done using a UV-visible spectrophotometer.

2.6.5. Effect of Temperature. To determine how the temperature affects the adsorption process, batch experiments were conducted at 298, 303, 308, 313, 318, 323, 328, and 333 K at pH of 2, initial dye concentration of 10 mg/L, and 0.7 g VIFP biosorbent and agitated at 200 rpm for 180 min. The mixtures were centrifuged, and the supernatant was analysed for the remaining dye by UV-Vis spectrophotometer.

In this series of batch adsorption studies, the supernatant was analysed for the remaining CR dye concentration using a UV-visible spectrophotometer at a wavelength of maximum absorption of 499 nm for pH 5-10 and 564 nm for pH 2-4. All measurements were done in triplicate, and the mean values were provided along with an error estimate of standard deviation. The adsorption efficiency and capacity (q_e) were determined using

$$\begin{aligned} \%\text{of dye removal} &= \frac{[C_i - C_e]}{[C_i]} \times 100, \\ \text{Adsorption capacity, } q_e &= \frac{[C_i - C_e]}{m} \times V, \end{aligned} \tag{1}$$

where C_i is the initial CR dye concentration (mg/L), C_e is the CR dye concentration at equilibrium (mg/L), q_e is the amount of CR adsorbed (mg/g), V is the volume of CR dye (L), and m is the mass of the VIFP adsorbent (g).

2.6.6. Adsorption at Optimum Conditions. This procedure was carried out at all optimum conditions of pH 2, 0.7 g VIFP dosage, 180 min contact time, initial CR dye concentration of 10 mg/L at 328 K, and agitation of 200 rpm. Briefly, 50 mL of CR dye (10 mg/L) was measured and placed in a 250 mL Erlenmeyer flask, followed by the addition of 0.1 M HCl or 0.1 M NaOH for pH adjustment to 2. The solution was then contacted with 0.7 g of VIFP biosorbent for 180 min at 328 K, and the flasks were shaken at 200 rpm in an incubator shaker. After 180 min elapsed, the mixture was centrifuged and analysed for the remaining dye concentration by using a UV-Vis spectrophotometer. This procedure was carried out in triplicate.

2.7. Adsorption Isotherms. To elucidate the interaction between CR dye and VIFP adsorbent concerning the surface characteristics of the biosorbent and its affinity towards the adsorbate, this study employed the most common Freundlich and Langmuir isotherm models.

2.7.1. Freundlich Isotherm Model. The Freundlich isotherm assumes the presence of unlimited sorption sites on the adsorbent, suggesting an adsorption process which involves multilayer coverage of the adsorbate onto the surface of the adsorbent. It also explains the adsorbent's surface heterogeneity and the availability of binding sites having different activation energies. This isotherm model can explain the adsorption capacity and intensity of the adsorption process through

$$\log q_e = \log K_F + \frac{1}{n} \log C_e, \tag{2}$$

where q_e is the amount of adsorbate adsorbed per unit weight of adsorbent (mg/g), C_e is the equilibrium adsorbate concentration in solution (mg/L), and K_F and $1/n$ are the Freundlich constants representing the adsorption capacity (L/mg) and adsorption intensity, respectively. A plot of log q_e against C_e shows that the parameters K_F and n can be determined from the y-intercept and slope, respectively. Obtaining a smaller value of $1/n$ depicts better adsorption and stronger binding between the adsorbate and the surface of the adsorbent. The favourability of the adsorption can be inferred by values of n, whereby n values between 1 and 10 indicate favourable adsorption [27].

2.7.2. Langmuir Isotherm Model. The Langmuir isotherm assumes monolayer adsorption onto the adsorbent's site. This model suggests a dynamic equilibrium of the adsorption-desorption process. It explains further that the surface of the adsorbent is homogenous with binding sites of equivalent activation energy. This model can be explained through

$$\frac{1}{q_e} = \frac{1}{q_m} + \frac{1}{K_L q_m}\left(\frac{1}{C_e}\right), \tag{3}$$

$$R_L = \frac{1}{1 + K_L C_o}. \tag{4}$$

C_e and C_o represent the equilibrium and initial concentration of the adsorbate (mg/L), respectively, and q_e is the amount of adsorbate adsorbed (mg/g). Moreover, the Langmuir constant K_L entails the adsorption capacity (mg/g), while q_m is the maximum adsorption capacity (mg/g), and q_e represents the equilibrium adsorption capacity (mg/g). The q_m and K_L can be obtained by a linear plot of $1/C_e$ against $1/q_e$. The separation factor RL can be obtained in this model using Equation (4). The adsorption process is unfavourable when R_L is greater than 1, linear when $R_L = 1$, and irreversible when $R_L = 0$. For a favourable adsorption process, the value of R_L must be greater than 0 but less than 1 [28].

2.8. Adsorption Kinetic Models. The adsorption kinetic model provides insights into the mechanism of the adsorption process. The pseudo-first-order, pseudo-second-order, and intraparticle diffusion models were applied to describe the mechanism of CR dye adsorption onto VIFP adsorbent.

2.8.1. Pseudo-First-Order Kinetic Model. Equations (5) and (6) were used to fit the experimental data with a pseudo-first-order model:

$$\frac{d\mathrm{q}_t}{dt} = k_1(q_e - q_t), \tag{5}$$

$$\log (q_e - q_t) = \frac{(\log q_e - k_1 t)}{2.3.3}, \quad (6)$$

where q_t is the amount of adsorbate adsorbed per unit mass of adsorbent at time t (mg/g), k_1 is the pseudo-first-order rate constant (per min), and t is the contact time (min). A plot of $\log (q_e - q_t)$ against t determines the pseudo-first-order rate constant from the slope [29].

2.8.2. Pseudo-Second-Order. In pseudo-second-order adsorption, the rate-limiting step is chemisorptions which govern the nature of the adsorption. Pseudo-second-order adsorption kinetics can best be described by

$$\frac{dq_t}{dt} = k_2(q_e - q_t)^2, \quad (7)$$

$$\frac{t}{q_t} = \frac{1}{k_2 q_{e^2}} + \frac{t}{q_e}, \quad (8)$$

where k_2 and q_e are the pseudo-second-order rate constant (g/mg/min) and equilibrium adsorption capacity, respectively; these parameters are determined from a linear plot of t/q_t against time (min) [29, 30].

2.8.3. Intraparticle Diffusion Model. The intraparticle diffusion model is represented by Equation (9), and the values of the constants can be obtained from the plot of q_t vs $(t)^{1/2}$. In the equation, t is time (min), and k_{int} is the rate constant for intraparticle diffusion (mg/g $\text{min}^{-0.5}$).

$$q_t = k_{\text{int}}(t)^{1/2}. \quad (9)$$

2.9. Biosorption Thermodynamics. The thermodynamic parameters, namely, standard entropy change (ΔS°), Gibbs free energy change (ΔG°), and standard enthalpy change (ΔH°) presented in Equations (10), (11), and (12), were determined to illustrate the nature and feasibility of the adsorption process. The constant R represents the gas constant (kJ/mol K), and T is the absolute temperature (K) [31].

$$\Delta G\circ = \Delta H\circ - T\Delta S, \quad (10)$$

$$G\circ = -\text{RTI}nK_d, \quad (11)$$

$$InK_d = \frac{\Delta S\circ}{R} - \frac{\Delta H\circ}{RT}. \quad (12)$$

2.10. Desorption Studies. Desorption studies were crucial to ensure the reusability of the VIFP biosorbent, which in turn leads to the minimization of cost. For desorption experiments, the VIFP biosorbent that was used for the adsorption of 10 mg/L of the CR dye solution was centrifuged to separate the solution from the loaded biosorbent. The mixture was filtered by the Whatman filter paper, and the residue was washed with deionized water to remove traces of unadsorbed dye molecules. The biosorbent was then agitated with 50 mL deionized water while regulating pH at 2, 3, 4, 5, 6, 7, 8, 9, and 10 as before by using 0.1 M NaOH or HCl. The desorbed CR dye was determined using a UV-Vis spectrophotometer as the amount of dye remaining in the solution. The initial concentration of the adsorbed CR dye was 9.23 mg/L.

3. Results and Discussion

3.1. Characteristics of VIFP Biosorbent

3.1.1. XRD Analysis. The crystal structure of the VIFP biosorbent was examined by X-ray diffraction (Figure 2). For both untreated and acid-treated VIFP biosorbents, the typical XRD patterns show two broad peaks at $2\theta = 15.6^\circ$ and $2\theta = 21.7^\circ$. While the weak peak at $2\theta = 15.6^\circ$ was assigned to lignin and hemicelluloses [32], the strong peaks at $2\theta = 21.7^\circ$ are characteristic of cellulose as the dominant material in VIFP biosorbent [33]. The treatment of VIFP biosorbent with HNO_3 caused slight changes in the cellulose structure, manifested by the presence of more intense peaks in the acid-treated VIFP biosorbent than in the pristine material. This modification could contribute to more exposure of the functional groups, which play a vital role in the adsorption of environmental pollutants. Generally, structural analysis indicates that both crystalline and amorphous forms coexist in the VIFP material, characteristic of cellulose crystallinity [34].

3.1.2. BET Analysis. The specific surface area of the untreated and acid-treated VIFP biosorbent was determined by the BET (Brunauer-Emmett-Teller) method. The acid-treated VIFP biosorbent (1063.6791 m^2/g) had a much greater specific surface area (three times) than the untreated VIFP biosorbent (358.0724 m^2/g), as shown in Table 1. This implies the suitability of the treated VIFP biosorbent in accommodating more dye molecules on its surface than the untreated VIFP biosorbent. Likewise, the pore sizes of 15.2265 Å and 15.2773 Å were obtained for untreated and acid-treated VIFP samples, respectively. The pore volumes of untreated and acid-treated VIPF samples were estimated to be 1.4246 cm^3/g and 1.6837 cm^3/g, respectively. This enhancement of porosity characteristics of the VIFP material after treatment with 0.1 M HNO_3 is a good indicator of good performance towards the adsorption of dyes. Additionally, supplementary information Figure S1 shows type V isotherms with H3 hysteresis loop, which indicates that VIFP biosorbent is a mesoporous material. Additionally, H3 hysteresis observed for VIFP biosorbent represents materials which produce slit-shaped pores and do not display any limiting adsorption at elevated relative pressure [35].

3.1.3. SEM Analysis. The surface characteristics of the adsorbent before and after acid treatment were characterised by SEM. The SEM micrographs of the pristine VIFP material (Figure 3(a)) showed irregular and porous heterogeneous surfaces. The SEM image of the acid-treated VIFP biosorbent (Figure 3(b)) displays improvement in the porous nature of the material. Pores of various sizes, cracks, and cavities were formed after acid treatment. The adsorption process and how the dye molecules diffuse into the interior space of VIFP particles are aided by this significant enhancement in surface characteristics. The change in the porous nature of the biosorbent could be attributed to the reaction of cellulose components in the biosorbent with HNO_3.

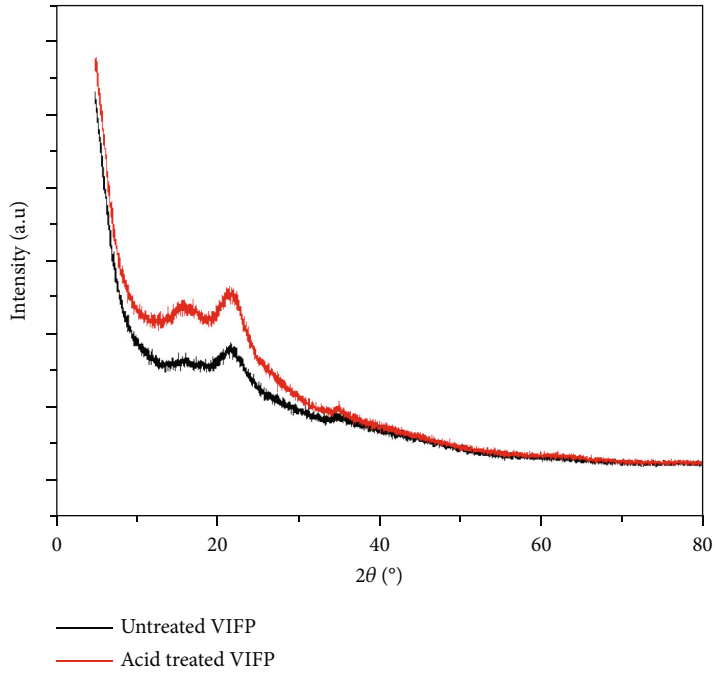

Figure 2: XRD profile of untreated and acid-treated VIFP biosorbent.

Table 1: BET analysis parameters for untreated and treated VIFP biosorbents.

Sample	Specific surface area (m^2/g)	Pore radius (Å)	Total pore volume (cm^3/g)
Untreated VIFP	358.0724	15.2265	1.4246
Treated VIFP	1063.6791	15.2773	1.6837

Moreover, acid treatment results in the oxidation of the cellulose in the carbonaceous material, exposing the binding sites for easy diffusion of the dye molecules [36].

3.1.4. TEM Analysis of the VIPF Biosorbent. Further investigation of the adsorbent morphological features was studied using TEM. The TEM images of both untreated (Figure 4(a)) and acid-treated (Figure 4(b)) VIFP biosorbents show quasispherical particles. While most of the particles in the pristine VIPF material are highly agglomerated, the acid-treated VIFP biosorbent is somewhat separated. In addition, the TEM image of the untreated biosorbent displays a compact dark material ascribed as a carbonaceous material. At the same time, the carbonaceous particles in the acid-treated VIFP biosorbent appear to be somewhat clear and well dispersed.

3.1.5. FT-IR Analysis of the VIPF Biosorbent. FT-IR spectral signatures for the untreated VIPF biosorbent in Figure 5 show a broad peak at 3272 cm^{-1} due to O-H stretching vibration of hydrogen-bonded hydroxyl groups that can be attributed to carboxyls, phenols or alcohols, and water. The peak at 2921 cm^{-1} shows the presence of C-H stretching vibrations in the cellulose unit. Peaks at 1729, 1436, and 1231 cm^{-1} arise from the hemicellulose unit. The peak at 1729 cm^{-1} is due to C=O stretching vibration due to esters, aldehydes, or ketones. The vibration peak at 1436 cm^{-1} is due to H-CH and O-CH in-plane bending vibration, and that occurring at 1231 cm^{-1} corresponds to COH bending at C6. A small peak at 1603 cm^{-1} corresponds to C=C stretching, which may be due to the aromatic moieties present in the material. The aromatic skeletal vibrations recorded at 1533 cm^{-1} are reported to have originated from the lignin unit. Also, a peak at 1316 cm^{-1} may be due to CH_2 rocking vibration at C6, and it may also show the presence of COO^- symmetric stretching vibration. The sharp peak at 1017 cm^{-1} depicts the presence of C-O groups that arises due to acids, phenols, esters, aromatic compounds, and alcohol [37].

After acid treatment, the IR spectrum presented in Figure 5 shows crucial changes in the adsorbent's structure, manifested by the disappearance and shifting of the peaks to higher or lower wave numbers. This observation indicates that the acid treatment facilitated the dissolution of lignin and hemicellulose units. These changes, along with the oxidation of C6 due to acid treatment, could have impacted significant changes in the porosity of the biosorbent. The O-H stretching vibration peak shifted from 3272 to 3350 cm^{-1}. This shift can be ascribed to the modifications at C6 in converting the primary hydroxyl group to the carboxyl group, as illustrated in Figure 5. More notable changes in the intensity and position of the absorption peaks were also apparent for the peaks at 2921, 1729, 1603, 1316, 1231, and 1017 cm^{-1} which shifted to 2928 cm^{-1}, 1720, 1624, 1320, 1228, and

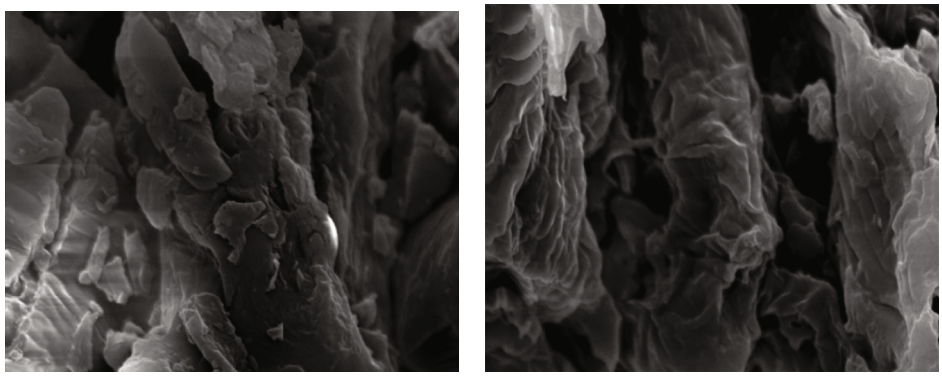

(a) (b)

Figure 3: SEM images for (a) untreated VIFP sample and (b) acid-treated VIFP samples at a magnification of 10,000x.

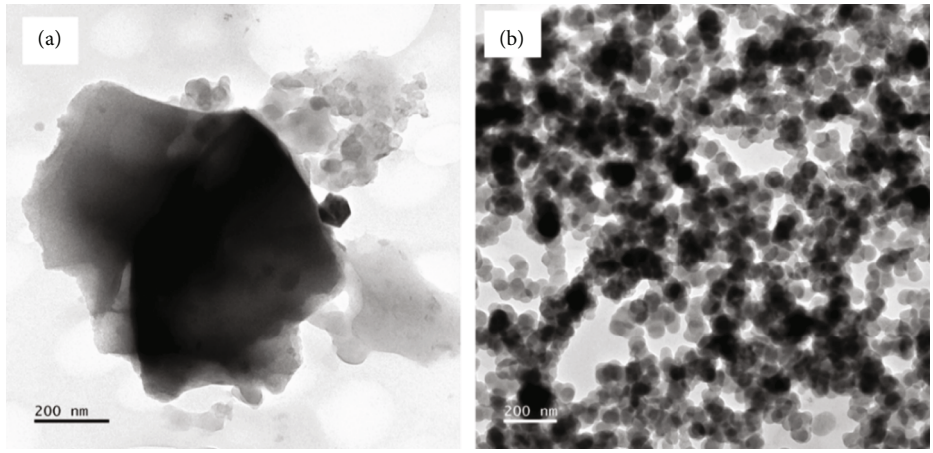

Figure 4: TEM images for (a) untreated VIFP and (b) acid-treated VIFP biosorbent.

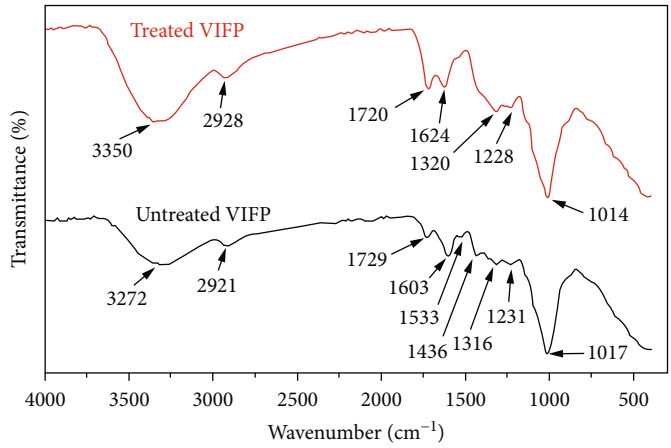

Figure 5: FT-IR spectra of untreated and acid-treated VIFP biosorbent.

1014 cm^{-1}, respectively. The disappearance of absorption peaks at 1533 and 1436 cm^{-1} was also noted. It was further revealed that following acid treatment, the intensity of the peaks responsible for the hemicelluloses unit decreased while some of them vanished. In addition, the peak at 1533 cm^{-1} that arises from the lignin unit disappeared in the acid-treated VIFP biosorbent. This observation further suggests that acid treatment influenced the removal of impurities, oxidation at C6, and exposing functional groups responsible for binding pollutants. Sharma et al. reported similar results in preparing

carboxy cellulose nanofibers from untreated biomass using nitric acid alone and a combination of nitric acid with sodium nitrite [36]. Supplementary information Figure S3 further explains the proposed mechanism for the adsorption process of CR dye by VIFP biosorbent [37]. At the acidic pH of the solution, the CR molecule dissociates to give polar groups of R-SO_3^-, NH_2, and -N=N- groups which become protonated.

Similarly, at the same pH, the surface groups of the biosorbent, such as -COOH and -OH, become protonated to -$COOH_2^+$ and OH_2^+, respectively. This creates room for hydrogen bonding between the oxygen-containing groups of the biosorbent (-$COOH_2^+$ and OH_2^+) with the nitrogen-containing group on the CR molecule ($^+NH_2$ and -$^+$N=N-). Also, electrostatic interaction is expected between the -SO_3^- of the CR molecule and -$COOH_2^+$ on the surface of the biosorbent.

3.1.6. Point of Zero Charge (pzc). The biosorption of environmental pollutants from an aqueous solution depends on the nature of the contaminant being removed and the surface chemistry of the biosorbent. The relationship between biosorbent surface chemistry and pollutant nature can best be described by the point of zero charge (pH_{pzc}). Generally, pH_{pzc} zero implies that the biosorbent surface has no charge. The point of zero charge of the VIFP biosorbent was found to be 6.42 (Figure 6) in this investigation, indicating that the surface of the VIFP biosorbent is negatively charged above this pH and positively charged below this pH. The pH below this value results in protonation of the surface of the VIFP biosorbent, which facilitates strong electrostatic interaction with the negatively charged ions in the dye. The isoelectric point of CR dye is 3, and at any pH below this point, it exists in its molecular form, while at pH above, it exists in its dissociative nature. Therefore, CR dye is expected to be negatively charged at a pH greater than 4. This, in turn, causes the repulsion of the negatively charged CR ions with the negatively charged surface at high pH.

3.2. Batch Adsorption Studies. This study investigated the biosorption of CR dye by VIPF via a batch system. Evaluation of the adsorption capacity and the rate of adsorption of CR dye onto VIFP biosorbent was performed at different initial CR dye concentrations, solution pH, VIFP dosage, contact time, and temperature.

3.2.1. Effect of pH. To evaluate the effect of pH on the removal of CR dye by VIFP biosorbent, studies were carried out in the pH range of 2-10. The results (Figure 7) show that the maximum adsorption occurred in an acidic environment. The high adsorption efficiency of 78% at pH 2 can be substantiated by the surface charge of the biosorbent, which is preferentially protonated in acidic media. In an acidic medium, adsorption is mostly favoured due to a positively charged surface interacting strongly with the anionic dye. Generally, the positive charge acquired on the surface can be elucidated by the Henderson-Hasselbalch equation ($pH = pKa + \log([\text{conjugate base}]/[\text{weak acid}])$), which shows the relationship between pH and pKa. It has been reported that the −COOH group presents a pKa value of approximately 4.5

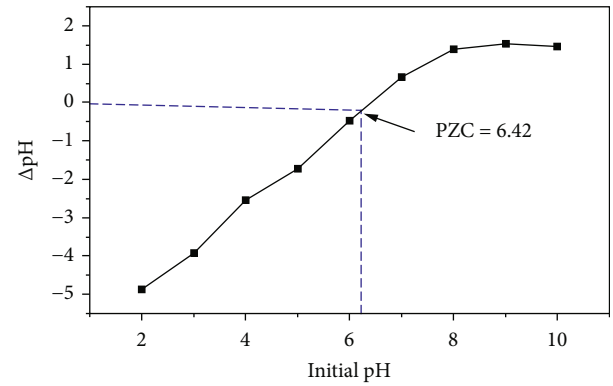

Figure 6: Point of zero charge of the VIFP biosorbent.

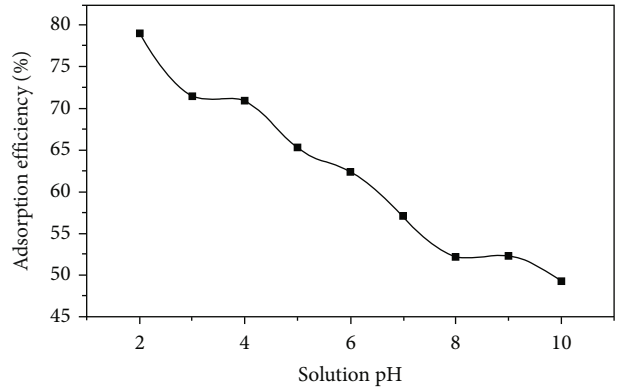

Figure 7: Effect of pH on CR dye uptake by VIFP biosorbent (0.7 g of VIFP, 50 mg/L initial CR concentration, and contact time of 180 min at 298 K).

[38]. When pH is lower than pKa, ($pH < pKa$), this group carries a positive charge which results from a strong electrostatic interaction between the negatively charged SO_3^- group of dye and the positively charged surface. Another interaction existing is hydrogen bonding between the dye groups with nitrogen (amine (−NH_2) and azo (−N=N−)) and oxygen from the surface groups of the VIFP biosorbent. It was further observed that the efficiency of the VIFP biosorbent towards removing CR dye decreased with the increase in solution pH. At higher pH (basic condition), the functional groups are said to be anionic. For instance, the carboxylic groups (−COOH) of the biosorbent completely ionize to COO− at higher pH. This leads to interionic repulsion between the negatively charged ions of the dye and the biosorbent, which decreases the adsorption efficiency [37]. Moreover, the decrease in adsorption efficiency as the pH increases is due to the accumulation of excess OH^- ions in the solution, which compete for the adsorption sites [39]. Various studies have also reported a similar trend in the adsorption of CR dye using coir pith, Phoenix dactylifera seeds, and activated carbon [39–41].

3.2.2. Effect of VIFP Biosorbent Dosage. For catalytic activity, the amount of VIFP biosorbent is another significant component since it substantiates the amount of CR dye that a

specified mass of adsorbent can adsorb. The effect of VIFP biosorbent dosage (0.1-0.9 g) on the adsorption of CR dye is shown in Figure 8. The trend shows that the adsorption of CR dye is enhanced as the biosorbent dosage increases from 0.1 to 0.7 g. This increase in adsorption efficiency from 75.94% for 0.1 g to 99.74% for 0.7 g is due to increased VIFP surface binding sites that facilitate the interaction with the ions in the dye. This is obvious because the increase in biosorbent dosage occurs at constant dye molecules in the solution (fixed concentration), giving a high possibility of creating more binding sites than the available adsorbate molecules. Consequently, some of the binding sites remain unoccupied. It was also established from the BET, SEM, and FT-IR results that acid treatment increases the porous nature of the biosorbent, which in turn exposes the binding sites of cellulose unit (-OH and COOH groups) that are responsible for binding CR dye molecules. When the VIFP dosage was increased to 0.9 g, the absorption efficiency decreased, which is attributed to aggregation, which impedes further access to adsorption sites. Therefore, the maximum adsorption efficiency of 99.74% obtained with 0.7 g of VIFP was considered the optimum dosage for other experiments. The trend of adsorption efficiency as a function of VIFP dosage agrees well with that reported by Pathania et al., who achieved maximum adsorption of 84% with a biosorbent dosage of 0.6 g [40]. This study's results also relate to those of Vimonses et al., in which clay materials were used to remove CR dye, recording an increase in adsorption efficiency from 18 to 100% and 12 to 95% for kaolin and zeolite adsorbents, respectively [28].

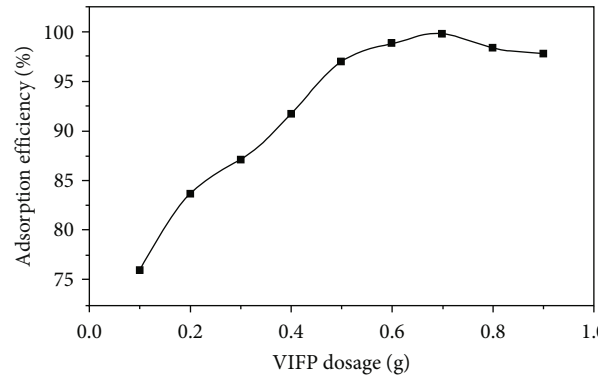

Figure 8: Effect of VIFP biosorbent dosage on CR dye adsorption (pH 2, 50 mg/L initial CR concentration, and contact time of 180 min at 298 K).

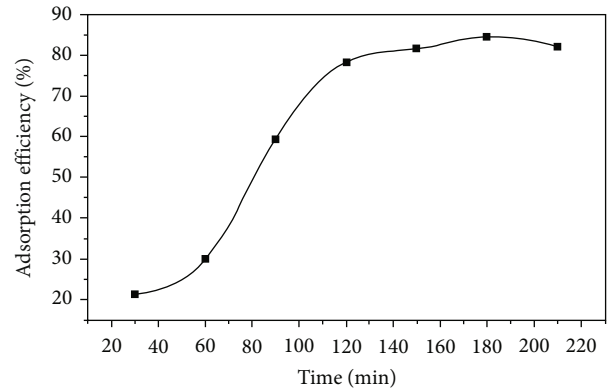

Figure 9: Effect of contact time on adsorption of CR dye by VIFP (pH 2, 0.7 g VIFP, and 50 mg/L initial CR concentration at 298 K).

3.2.3. Effect of Contact Time. The influence of contact time on the adsorption of CR dye was investigated in the range of 30 –210 min at pH = 2, a temperature of 298 K, a dye concentration of 50 mg/L, and a VIFP dose of 0.7 g. The results in Figure 9 show the sharp adsorption of CR dye at the initial stages due to abundant binding sites and sufficient surface area of the acid-treated VIFP adsorbent. Generally, the results indicate that the adsorption efficiency rapidly increased from 21.46 to 84.47% as the contact time varied from 30 to 180 min. This conclusion is supported by Namasivayam and Kavitha [39]. This swift increase in CR dye uptake at the outset can be linked to active sites on the VIFP surface. However, the adsorption efficiency decreased when the contact time was increased to 210 min. This is because, after 180 minutes of adsorption, the available vacant active sites were crowded by CR dye molecules, leading to repulsion between dye molecules on the VIFP biosorbent and those present in the solution.

Consequently, the repulsive force causes a reduction in the quantity of dye to be adsorbed [42]. Therefore, the optimum contact time for the adsorption of CR dye on VIFP adsorbent was achieved at 180 min. A similar trend was achieved by Chukki et al. [43] in their studies on the removal of CR dye by using *Chrysanthemum indicum* microparticles.

3.2.4. Effect of Initial CR Dye Concentration. The results in Figure 10 depict that the adsorption efficiency behaves inversely with the initial CR dye concentration. The adsorption efficiency decreases as the initial CR dye concentration increases. Due to the copious adsorption sites on the surface of the adsorbent, the adsorption process was favoured at low dye concentrations. The higher adsorption efficiency of 99.74% was achieved at a CR dye concentration of 10 mg/L, which was then reduced to 96.6% at a CR dye concentration of 80 mg/L. This decreasing efficiency at higher CR dye concentrations is due to the saturation of the fixed number of VIFP active sites. At high concentrations, dye molecules tend to aggregate, forming more giant micelles, which decrease the diffusion of the ions into the surface sites of the biosorbent. The trend remained the same at different temperatures. Since the maximum adsorption was attained at 10 mg/L, this value was taken as the optimum initial dye concentration. A similar observation was reported by Lafi et al. on the removal of CR dye using adsorbents prepared from *Phoenix dactylifera* seeds [37]. Variation of adsorption efficiency of VIFP biosorbent with initial CR dye concentration yielded a similar trend at different temperatures. However, the adsorption of CR dye was observed to be favoured with increasing temperature.

3.2.5. Effect of Temperature. The investigation of the effect of solution temperature on the adsorptive removal of CR dye from aqueous solution was performed at a temperature

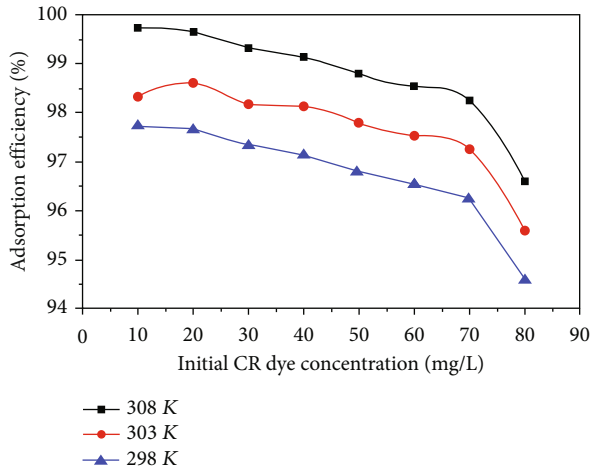

Figure 10: Effect of initial dye concentration on CR dye uptake by VIFP biosorbent (pH 2, 0.7 g VIFP dosage, and contact time of 180 min at 298-308 K).

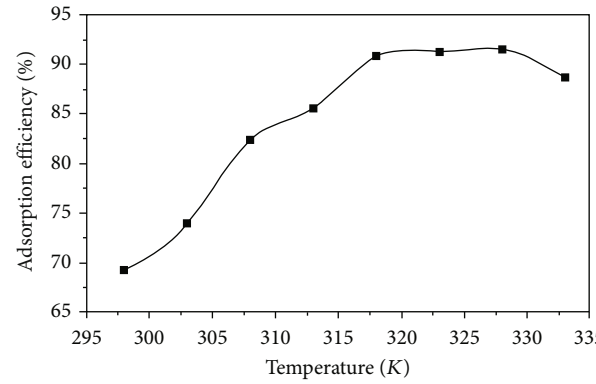

Figure 11: Effect of temperature on CR dye adsorption by VIFP biosorbent (pH 2, 0.7 g of VIFP, 10 mg/L initial CR concentration, and contact time of 180 min).

interval of 298 K to 333 K. Other experimental variables were kept at an optimum level of pH 2, VIFP dosage of 0.7 g, contact time of 180 min, and initial CR dye concentration of 10 mg/L. The results in Figure 11 indicate that increasing the temperature from 298 K to 333 K increased the removal efficiency from 69.26 to 91.46%. This observation justifies the endothermic nature of the adsorption of CR dye by VIFP biosorbent. This means that a supply of energy from the surrounding is required to achieve high adsorption of CR dye. Maximum adsorption was evident at 328 K, implying that at this particular temperature, more dye molecules were diffused across the extrinsic boundary and internal pores of the surface of the VIFP biosorbent. However, when the temperature was increased beyond 328 K, the adsorption efficiency was reduced. These results corroborate those reported by Amar et al. who utilized Mg-doped $CoFe_2O_4$ nanoparticles to remove CR dye from aqueous solutions [9].

3.3. Adsorption Isotherm Models. The equilibrium adsorption isotherm models play important roles in designing the adsorption systems and understanding the interaction pattern between the adsorbent and adsorbate. In this study, we have employed the most common Langmuir and Freundlich isotherm models to get an insight into the interaction of CR dye with VIFP biosorbent at equilibrium. The Freundlich isotherm model describes the multilayer coverage of the adsorption processes ascribed to the presence of a heterogeneous adsorbent system. From the linear form of the Freundlich model (Equation (2) and Figure 12(a)), the values of K_F and n parameters (Table 2) were determined, which offer insight into the extent of adsorption and the heterogeneity of the adsorbent, respectively. Furthermore, the value of n was found to be 1.54, depicting the favourability of the adsorption process. This is because the value n conforms to the relation $1 < n < 10$, and it has been established that, for a favourable adsorption process, the values of n should be in the range of 1-10 [44].

On the other hand, the Langmuir model has based on the premise that adsorption occurs at particular homogenous binding sites within the adsorbent. Equation (3) was used to plot Figure 12(b), which was then utilized to obtain the data displayed in Table 2, i.e., q_m, K_L,R^2, and R_L, which represent the maximum adsorption capacity, the maximum affinity of the biosorbent binding sites, correlation coefficient, and equilibrium factor, respectively. The feasibility of the adsorption process was deduced by the values of the separation factor, R_L, and was obtained by manipulating Equation (4). In principle, the value of the separation factor, $0 < \mathrm{RL} < 1$, represents a favourable adsorption process. In this study, the value of R_L was found to be 0.83, which is less than 1 but greater than 0, signifying favourable CR dye adsorption by VIFP biosorbent. As a result, the maximum adsorption capacity (q_m) for the uptake of CR dye molecules on VIFP obtained from the Langmuir isotherm was 7.91 mg/g. From this point of view, each CR-VIFP adsorption had equivalent adsorption activation energy, and there was monolayer coverage of CR molecules on the surface of the biosorbent. In addition, the correlation coefficient (R^2), which describes the favourability of the Langmuir and Freundlich models to the experimental data, was also determined. The Langmuir isotherm model recorded a higher correlation coefficient, R^2 (0.97918), than the Freundlich model (0.94235), as shown in Table 2. This implies that the Langmuir model better explains the experimental data for the adsorption of CR onto VIFP biosorbent than the Freundlich model. This further infers that there was a monolayer fitting of the CR dye molecule on the surface of the VIFP biosorbent.

3.4. Biosorption Kinetic Studies. Determination of biosorption kinetics was important to get insight into the potential biosorption mechanism, reaction pathway, and the time taken for the process to attain equilibrium. Three kinetic models were employed to fit the experimental results: pseudo-first-order, pseudo-second-order, and intraparticle diffusion. The pseudo-first-order kinetic model assumes that physisorption plays the leading part in the biosorption process. With the help of pseudo-first-order Equations (5) and (6), the plot of $\log(q_e - q_t)$ vs. t was obtained, while

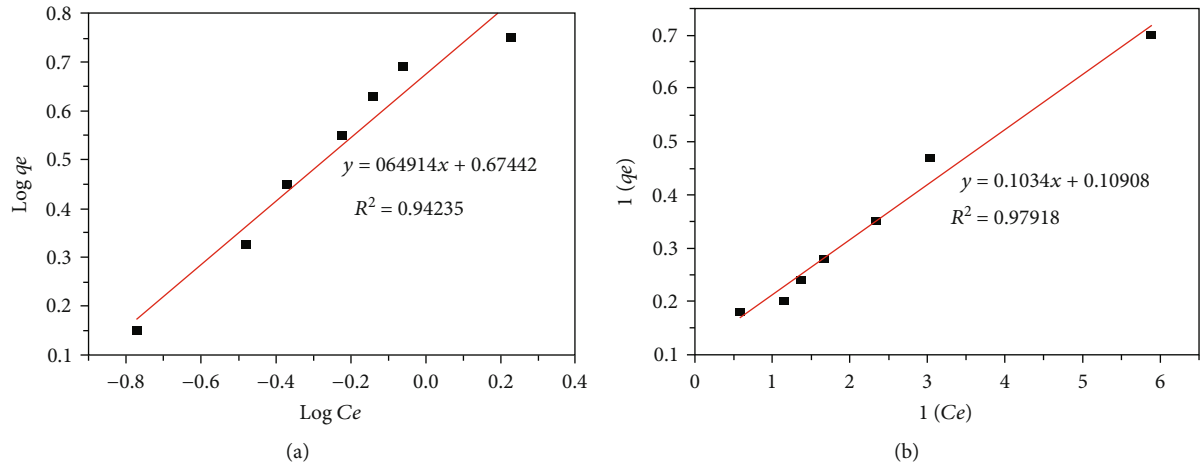

Figure 12: (a) Freundlich and (b) Langmuir isotherms for CR dye uptake onto treated VIFP (pH 2, 0.7 g of VIFP, initial CR concentration of 20-80 mg/L, and contact time of 180 min at 298 K).

Table 2: Freundlich and Langmuir isotherm parameters for CR dye adsorption by VIFP.

Freundlich parameters				Langmuir parameters				
K_F	n	R^2	±SD	q_m	K_L	R^2	±SD	R_L
4.73	1.54	0.94235	0.0131	7.91	0.01	0.97918	0.0035	0.83

pseudo-second-order Equations (7) and (8) were used to obtain a plot of t/q_t vs. time min) [45]. The correlation coefficient for the pseudo-first-order was found to be 0.96051, while that of the pseudo-second-order was 0.9997, as shown in Figures 13(a) and 13(b) and Table 3. The lower correlation coefficient, R^2, for the pseudo-first-order (0.9605) compared to that obtained for the pseudo-second-order (0.9997) suggests that the pseudo-first-order kinetic model is not an ideal fit to explain the adsorption process. Therefore, in this study, pseudo-second-order best explains the adsorption process, indicating that both the adsorbate and the biosorbent determine the mechanism of the adsorption process. The calculated values of q_e in the pseudo-second-order kinetic model correspond to the experimental values, signifying a better fit of CR dye adsorption data into pseudo-second-order kinetics. Similar findings have been recounted on the adsorption of environmental pollutants by using different adsorbents [46–49].

Furthermore, the intraparticle diffusion model was employed to better understand the underlying adsorption mechanism and the rate-determining step. From Equation (9), the intraparticle diffusion model suggests that if by plotting q_t versus $t^{0.5}$ yields a linear graph passing through the origin, then intraparticle diffusion is the only rate-limiting step of the adsorption process. Figure 13(c) shows that the plot of q_t versus $t^{0.5}$ is not linear over the whole range of time and did not pass through the origin. The plot is evidently separated into three linear portions, signifying the multistages of the adsorption process. Since none of the three regions of the plot gave a linear straight line segment passing through the origin, the intraparticle diffusion is involved in the adsorption process but not the only rate-controlling step. This further indicates that film diffusion and intraparticle diffusion occurred simultaneously. The rate of adsorption of CR dye onto VIFP biosorbent may be controlled by other mechanisms such as complexation or ion exchange which may be operating concurrently [50]. Therefore, the mechanism of CR dye removal from aqueous phase by adsorption is assumed to consist of several steps including migration of the dye molecules from the bulk solution to the surface of the sorbent, diffusion through the boundary layer to the surface of the sorbent, and adsorption at sites and intraparticle diffusion into the interior of the biosorbent [51]. The parameters for interparticle diffusion model are shown in Table 3.

3.5. Biosorption Thermodynamics. Important parameters such as a change in the Gibbs free energy (ΔG°), change in enthalpy (ΔH°), and change in entropy (ΔS) were employed in explaining the thermodynamics of the adsorption process. These parameters were determined using Equations (10), (11), and (12) and are presented in Table 4. The standard ΔH° and ΔS were obtained from the plot of $\ln k_d$ against $1/T(K^{-1})$, as shown in Figure 14, in which ΔH° is obtained from the slope and ΔS from the y-intercept of the plot.

The results presented in Table 4 show a positive value of ΔH° (41.42 kJ/mol), which indicates the endothermic nature of the adsorption of CR dye by VIFP biosorbent. Also, the positive value of ΔS° (158.32 J/mol.K) reflects a spontaneous biosorption of CR dye. This value of ΔS° manifests a rise in the randomness between the sorbate and solution during the adsorption process [52]. Additionally, the spontaneity of the CR dye biosorption is equally aided by the values of free energy at different temperatures. The negative values

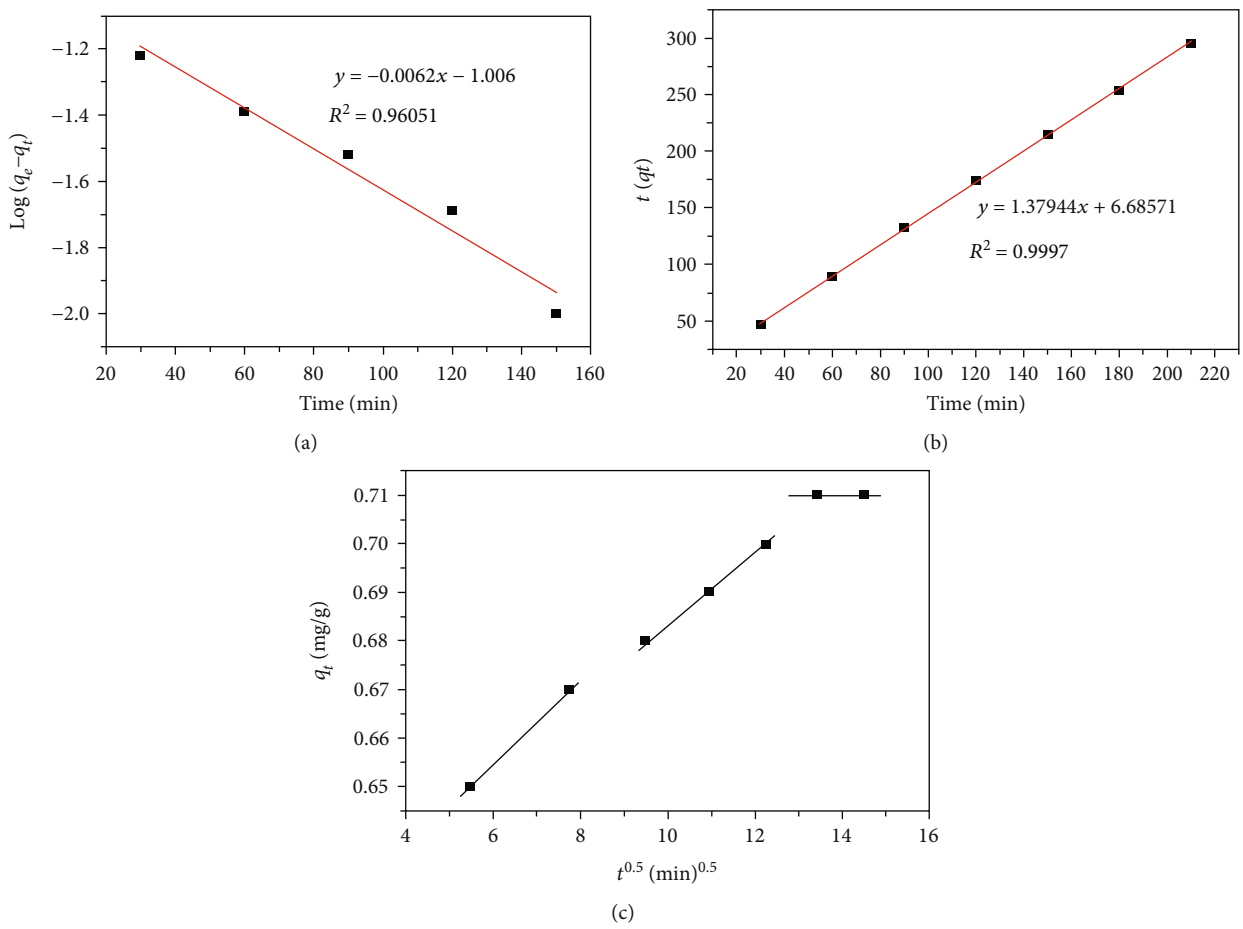

Figure 13: (a) Pseudo-first- and (b) pseudo-second-order kinetics and (c) intraparticle diffusion model for CR dye uptake by treated VIFP (pH 2, 0.7 g VIFP, contact time of 30-210 min, and initial CR concentration of 10 mg/L).

Table 3: Pseudo-first- and pseudo-second-order and intraparticle diffusion kinetic parameters for adsorption of CR by treated VIFP (pH 2, 0.7 g VIFP, contact time of 30-210 min, and initial CR concentration of 10 mg/L).

Q_e (exp.)	Pseudo-first-order kinetics				Pseudo-second-order kinetics				Intraparticle diffusion		
(mg/g)	k_1 (min^{-1})	q_e (cal.) (mg/g)	R^2	±SD	k_2 g/mg/min)	q_e (cal.) (mg/g)	R^2	±SD	k_{int} (mg/g$min^{0.5}$)	R^2	±SD
0.710	0.014	0.168	0.9605	0.104	0.390	0.706	0.9997	0.035	6.69×10^{-3}	0.979	0.009

Table 4: Calculated thermodynamic parameters (pH 2, 0.7 g of VIFP, contact time of 180 min, and initial CR concentration of 10 mg/L at a temperature range of 298-328 K).

ΔG° (kJ/mol)							ΔH°(kJ/mol)	ΔS°(kJ/mol.K)	R^2	±SD
298 K	303 K	308 K	313 K	318 K	323 K	328 K				
-5.78	-6.57	-7.37	-8.16	-8.95	-9.74	-10.53	41.42	158.32	0.9696	0.146

of ΔG°, -5.78, -6.57, -7.37, -8.16, -8.95, -9.74, and -10.53 kJ/mol at 298, 303, 308, 313, 318, 323, and 328 K, respectively, indicate that the biosorption of CR dye by VIFP biosorbent is thermodynamically favourable.

3.6. FT-IR Analysis for Acid-Treated VIFP before and after Adsorption of CR Dye. The FT-IR results presented in Figure 15 show the characteristic functional group of VIFP biosorbent before and after the adsorption of CR dye. The spectra show remarkable changes in the peak position of the VIFP biosorbent after the adsorption of CR dye. For example, a broad peak at 3350 cm^{-1}, which corresponds to the –OH stretching vibration of phenols and alcohols in lignin and cellulose of VIFP, shifted to 3335 cm^{-1} after the adsorption process. Other peaks in the spectrum of acid-treated VIFP before CR dye adsorption are 2928, 1624, 1320, and 1014 cm^{-1}, corresponding to $-CH_2$, –C=C, C–C, and C–O stretching, respectively. These peaks shifted to

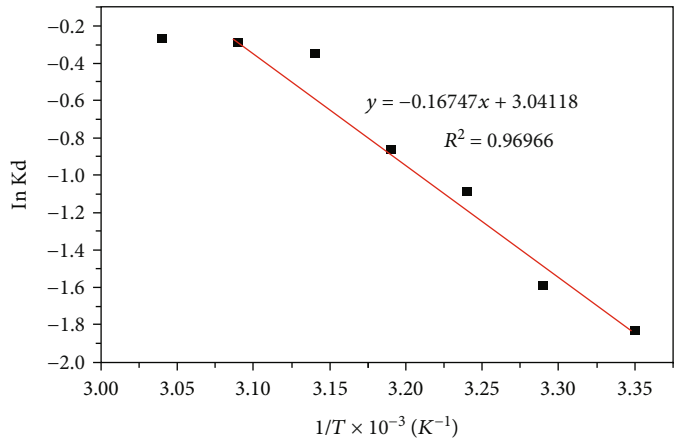

Figure 14: Thermodynamics for adsorption of CR by treated VIFP (pH2, 0.7 g VIFP, contact time of 180 min, and initial CR concentration of 10 mg/L at a temperature of 298-328 K).

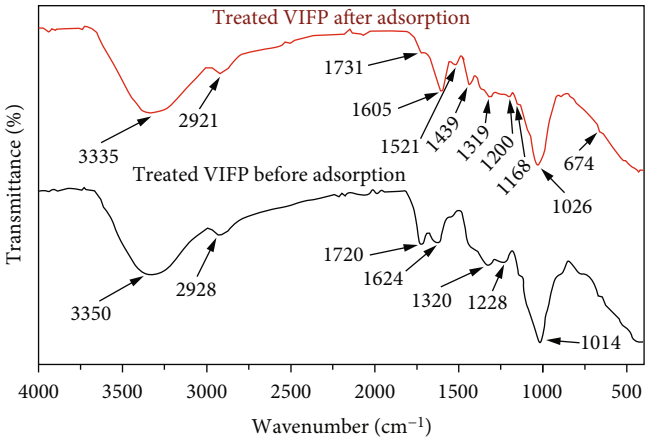

Figure 15: FT-IR spectra of acid-treated VIFP biosorbent before and after adsorption of CR dye.

2921, 1605, 1319, and 1026 cm^{-1}, respectively, after loading the VIFP biosorbent with CR dye. Also, the spectrum of acid-treated VIFP biosorbent after adsorption of CR dye exhibited new additional peaks at 1521, 1439, and 1168 cm^{-1}, indicating profound involvement of N=N stretching vibrations, C-N bending vibration, and –S=O stretching vibration of the SO_3 functional groups of the CR dye, respectively [53]. The observed changes in absorption bands and the emergence of new peaks affirm the adsorption of CR dye via electrostatic interactions of the functional groups in CR dye molecules with those of the VIFP biosorbent [54, 55]. These results corroborate with the findings of Jabar et al., on the removal of CR dye from aqueous solution using activated *Moringa oleifera* seed coat [56].

3.7. Comparison of Adsorption Efficiency of Untreated and Treated VIFP Biosorbent. To compare adsorption efficiency between untreated and acid-treated VIFP biosorbents, adsorption experiments were performed at optimum pH of 2, VIFP dosage of 0.7 g, contact time of 180 min, and initial CR dye concentration of 10 mg/L. The results in Table 5 show that untreated VIFP biosorbent recorded a low adsorption efficiency of 50.3% compared to 92.3% of the acid-treated VIFP biosorbent. The results agree with the BET results, which showed enhancement of porosity characteristics such as increased specific surface area, pore volume, and pore radius of the acid-treated VIFP biosorbent. Also, the FT-IR results presented in Figure 5 show crucial changes in the adsorbent's structure after acid treatment, including the dissolution of lignin and hemicellulose units and oxidation of C6. These changes could have contributed to significant changes in the porosity of the VIFP biosorbent, hence augmenting its adsorption behaviour. A similar observation was reported by Dawood and Sen, where untreated pine exhibited a low adsorption capacity of 32.65 mg/g compared to the acid-treated pine cone, which showed enhanced adsorption of 40.19 mg/g at the same experimental conditions [51].

3.8. Desorption Studies. A desorption study of the adsorbent is of paramount importance for the adsorption process to be economically viable. The results in Figure 16 show that as the solution pH increased, the desorption efficiency was also observed to augment. This suggests that the treatment of the loaded biosorbent with NaOH generated OH^- ions in the solution, which surrounded the carbon surface resulting in repulsive forces with the negatively charged ions of the CR dye, which in turn lowers the adsorption efficiency. It is also observed that a minimal amount of dye was desorbed, increasing very slightly throughout the desorption process. This indicates the strong interaction between CR dye molecules and the surface of the biosorbent. It also infers that the chemisorption mechanism prevailed in the adsorption process. Similar results were observed in Namasivayam and Kavitha's study on removing CR dye by coir pith [39].

3.9. Comparative Study. The extensive use of vast arrays of biosorbents is projected to necessitate many optimized and functional materials. A broad spectrum of the physicochemical process has recently been employed to prepare different biosorbents for environmental remediation. Previous studies

Table 5: Adsorption efficiency of untreated and acid-treated VIFP biosorbent (optimum pH of 2, initial CR dye concentration of 10 mg/L, VIFP dose of 0.7 g, and contact time of 180 min).

Sample	Initial concentration (mg/L)	Final concentration (mg/L)	SD	Adsorption (%)
Untreated VIFP	10	4.77	1.06	50.3
Acid-treated VIFP	10	0.77	0.64	92.3

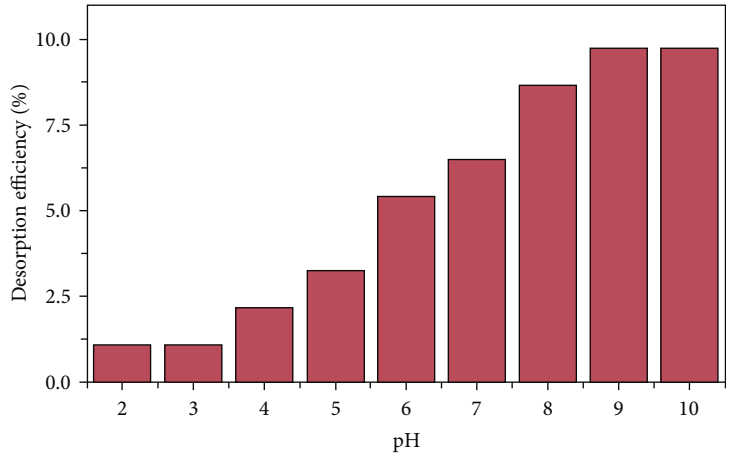

Figure 16: Effect of pH on desorption efficiency.

Table 6: Comparison of the performance of VIFP with other adsorbents on the removal of CR dye from aqueous solution.

Adsorbent	q_m (mg/g)	Adsorption efficiency (%)	Reference
Fly ash (50°C)	3.982	—	[57]
Activated carbon (50°C)	10.70	—	[57]
Chir pine (*Pinus roxburghii*) sawdust	5.8	72	[58]
Eucalyptus (*Eucalyptus globulus*) sawdust	—	>80	[59]
Fir (Abies nordmanniana) sawdust	28.1	86	[60]
Cabbage waste powder	2.313	91	[61]
Ag_2O–Al_2O_3–ZrO_2	333.32	38-89	[62]
ZnO@Ze composite	161.3	90	[12]
Vangueria infausta	7.91	92.3	Present study

have demonstrated the applicability of various biosorbents prepared from varying forms of biomass (Table 6). The efficiencies of the reported biosorbents differ depending on the type of biomass used, preparation procedure, experimental conditions, and nature of the pollutant being removed. The results obtained in this study have demonstrated that VIFP biosorbent recorded higher adsorption efficiency, similar to those reported in previous studies. Table 6 shows a comparison of the adsorption efficiency of VIFP biosorbent relative to other adsorbents reported in previous studies.

4. Conclusion

This study demonstrates that the acid-treated biosorbent prepared from *Vangueria infausta* fruit pericarp is suitable for removing Congo red dye in wastewater. At optimum pH of 2, biosorbent dosage of 0.7 g, initial dye concentration of 10 mg/L, contact time of 180 minutes, and temperature of 328 K, the maximum efficiency of 92.3% was achieved for the acid-treated VIFP biosorbent. The adsorption process in this study was spontaneous and is well described by the Langmuir adsorption isotherm and pseudo-second-order kinetics. These results assert that *Vangueria infausta* fruit pericarp could be sustainably used as a biosorbent in small-scale or large-scale wastewater treatment plants to remove dyes.

Data Availability

All the data used to support the findings of this study is included in the article.

Conflicts of Interest

The authors declare that there is no conflict of interest with respect to the research, authorship, and/or publication of this article.

Acknowledgments

The authors thank the management of the University of Dodoma for giving an opportunity to conduct this research as part of the MSc thesis of the first author under the supervision of the corresponding author.

Supplementary Materials

Figure S1: N_2 adsorption isotherm for untreated and acid-treated VIFP biosorbent. Figure S2: oxidation of C6 in cellulose by nitric acid. Figure S3: proposed interactions of CR dye and the surface of VIFP biosorbent. *(Supplementary Materials)*

References

[1] Y. Zhou, J. Lu, Y. Zhou, and Y. Liu, "Recent advances for dyes removal using novel adsorbents: a review," *Environmental Pollution*, vol. 252, Part A, pp. 352–365, 2019.

[2] M. T. Yagub, T. K. Sen, S. Afroze, and H. M. Ang, "Dye and its removal from aqueous solution by adsorption: a review," *Advances in Colloid and Interface Science*, vol. 209, pp. 172–184, 2014.

[3] S. K. Sen, S. Raut, P. Bandyopadhyay, and S. Raut, "Fungal decolouration and degradation of azo dyes: a review," *Fungal Biology Reviews*, vol. 30, no. 3, pp. 112–133, 2016.

[4] N. P. Raval, P. U. Shah, and N. K. Shah, "Adsorptive amputation of hazardous azo dye Congo red from wastewater: a critical review," *Environmental Science and Pollution Research*, vol. 23, no. 15, pp. 14810–14853, 2016.

[5] M. R. Abukhadra, A. Adlii, and B. M. Bakry, "Green fabrication of bentonite/ oxide composite (BE/) of enhanced adsorption and advanced oxidation removal of Congo red dye and Cr (VI) from water," *International Journal of Biological Macromolecules*, vol. 126, pp. 402–413, 2019.

[6] V. Katheresan, J. Kansedo, and S. Y. Lau, "Efficiency of various recent wastewater dye removal methods: a review," *Journal of Environmental Chemical Engineering*, vol. 6, no. 4, pp. 4676–4697, 2018.

[7] M. Shoaib, A. Ashar, Z. A. Bhutta, I. Muzammil, M. Ali, and A. Kanwal, "Biological methods for degradation of textile dyes from textile effluent," in *Development in Wastewater Treatment Research and Processes*, pp. 329–353, Elsevier, 2022.

[8] R. Liu, H. Fu, H. Yin, P. Wang, L. Lu, and Y. Tao, "A facile sol combustion and calcination process for the preparation of magnetic $Ni_{0.5}Zn_{0.5}Fe_2O_4$ nanopowders and their adsorption behaviors of Congo red," *Powder Technology*, vol. 274, pp. 418–425, 2015.

[9] I. A. Amar, J. O. Asser, A. S. Mady et al., "Adsorptive removal of Congo red dye from aqueous solutions using Mo-doped $CoFe_2O_4$ magnetic nanoparticles," *Pigment & Resin Technology*, vol. 50, no. 6, pp. 563–573, 2021.

[10] S. Moosavi, C. W. Lai, S. Gan, G. Zamiri, O. Akbarzadeh Pivehzhani, and M. R. Johan, "Application of efficient magnetic particles and activated carbon for dye removal from wastewater," *ACS Omega*, vol. 5, no. 33, pp. 20684–20697, 2020.

[11] M. Ali Khan, M. R. Siddiqui, M. Otero, S. A. Alshareef, and M. Rafatullah, "Removal of rhodamine b from water using a solvent impregnated polymeric dowex 5wx8 resin: statistical optimization and batch adsorption studies," *Polymers*, vol. 12, no. 2, p. 500, 2020.

[12] S. Madan, R. Shaw, S. Tiwari, and S. K. Tiwari, "Adsorption dynamics of Congo red dye removal using ZnO functionalized high silica zeolitic particles," *Applied Surface Science*, vol. 487, pp. 907–917, 2019.

[13] T. Zhang, W. Wang, Y. Zhao et al., "Removal of heavy metals and dyes by clay-based adsorbents: from natural clays to 1D and 2D nano-composites," *Chemical Engineering Journal*, vol. 420, article 127574, 2021.

[14] F. Sakr, S. Alahiane, A. Sennaoui, M. Dinne, I. Bakas, and A. Assabbane, "Removal of cationic dye (methylene blue) from aqueous solution by adsorption on two type of biomaterial of South Morocco," *Materials Today: Proceedings*, vol. 22, pp. 93–96, 2020.

[15] H. Saleem and S. J. Zaidi, "Developments in the application of nanomaterials for water treatment and their impact on the environment," *Nanomaterials*, vol. 10, no. 9, p. 1764, 2020.

[16] C. F. Schutte and W. Focke, *Evaluation of Nanotechnology for Application in Water and Wastewater Treatment and Related Aspects in South Africa*, Water Research Commission South Africa, 2007.

[17] H. Lu, J. Wang, M. Stoller, T. Wang, Y. Bao, and H. Hao, "An overview of nanomaterials for water and wastewater treatment," *Advances in Materials Science and Engineering*, vol. 2016, Article ID 4964828, 10 pages, 2016.

[18] M. N. Naseer, J. Jaafar, H. Junoh et al., "Metal-organic frameworks for wastewater decontamination: discovering intellectual structure and research trends," *Materials*, vol. 15, no. 14, p. 5053, 2022.

[19] V. S. Munagapati, J.-C. Wen, C.-L. Pan, Y. Gutha, J.-H. Wen, and G. M. Reddy, "Adsorptive removal of anionic dye (reactive black 5) from aqueous solution using chemically modified banana peel powder: kinetic, isotherm, thermodynamic, and reusability studies," *International Journal of Phytoremediation*, vol. 22, no. 3, pp. 267–278, 2020.

[20] S. Latif, R. Rehman, M. Imran, S. Iqbal, A. Kanwal, and L. Mitu, "Removal of acidic dyes from aqueous media using Citrullus lanatus peels: an agrowaste-based adsorbent for environmental safety," *Journal of Chemistry*, vol. 2019, Article ID 6704953, 9 pages, 2019.

[21] T. Jóźwiak, U. Filipkowska, S. Brym, and L. Kopeć, "Use of aminated hulls of sunflower seeds for the removal of anionic dyes from aqueous solutions," *International journal of Environmental Science and Technology*, vol. 17, no. 3, pp. 1211–1224, 2020.

[22] L. Gwatidzo, L. Chowe, C. Musekiwa, and N. Mukaratirwa-Muchanyereyi, "In vitro anti-inflammatory activity of Vangueria infausta: an edible wild fruit from Zimbabwe," *African Journal of Pharmacy and Pharmacology*, vol. 12, pp. 168–175, 2018.

[23] A. Maroyi, "Nutraceutical and ethnopharmacological properties of Vangueria infausta subsp. infausta," *Molecules*, vol. 23, no. 5, p. 1089, 2018.

[24] T. Aoki, T. Akashi, and S. I. Ayabe, "Flavonoids of leguminous plants: structure, biological activity, and biosynthesis," *Journal of Plant Research*, vol. 113, no. 4, pp. 475–488, 2000.

[25] J. K. Saka and J. D. Msonthi, "Nutritional value of edible fruits of indigenous wild trees in Malawi," *Forest Ecology and Management*, vol. 64, no. 2-3, pp. 245–248, 1994.

[26] F. Chigondo, B. C. Nyamunda, S. Sithole, and L. Gwatidzo, "Removal of lead (II) and copper (II) ions from aqueous solution by baobab (Adononsia digitata) fruit shells biomass," *IOSR Journal of Applied Chemistry*, vol. 5, no. 1, pp. 43–50, 2013.

[27] P. D. Saha, S. Chowdhury, M. Mondal, and K. Sinha, "Biosorption of direct red 28 (Congo red) from aqueous solutions by eggshells: batch and column studies," *Separation Science and Technology*, vol. 47, no. 1, pp. 112–123, 2012.

[28] V. Vimonses, S. Lei, B. Jin, C. W. Chow, and C. Saint, "Kinetic study and equilibrium isotherm analysis of Congo red adsorption by clay materials," *Chemical Engineering Journal*, vol. 148, no. 2-3, pp. 354–364, 2009.

[29] H. Moussout, H. Ahlafi, M. Aazza, and H. Maghat, "Critical of linear and nonlinear equations of pseudo-first order and pseudo-second order kinetic models," *Karbala International Journal of Modern Science*, vol. 4, no. 2, pp. 244–254, 2018.

[30] E. Bulut, M. Özacar, and İ. A. Şengil, "Equilibrium and kinetic data and process design for adsorption of Congo red onto bentonite," *Journal of Hazardous Materials*, vol. 154, no. 1-3, pp. 613–622, 2008.

[31] S. Lombardo and W. Thielemans, "Thermodynamics of adsorption on nanocellulose surfaces," *Cellulose*, vol. 26, no. 1, pp. 249–279, 2019.

[32] J. K. Fatombi, S. A. Osseni, E. A. Idohou et al., "Characterization and application of alkali-soluble polysaccharide of Carica papaya seeds for removal of indigo carmine and Congo red dyes from single and binary solutions," *Journal of Environmental Chemical Engineering*, vol. 7, no. 5, article 103343, 2019.

[33] J. Ma, L. Hou, P. Li, S. Zhang, and X. Zheng, "Modified fruit pericarp as an effective biosorbent for removing azo dye from aqueous solution: study of adsorption properties and mechanisms," *Environmental Engineering Research*, vol. 27, no. 2, 2022.

[34] W. Zhang, G. Zeng, Y. Pan et al., "Properties of soluble dietary fiber-polysaccharide from papaya peel obtained through alkaline or ultrasound-assisted alkaline extraction," *Carbohydrate Polymers*, vol. 172, pp. 102–112, 2017.

[35] K. S. Sing, "Reporting physisorption data for gas/solid systems with special reference to the determination of surface area and porosity (recommendations 1984)," *Pure and Applied Chemistry*, vol. 57, no. 4, pp. 603–619, 1985.

[36] P. R. Sharma, R. Joshi, S. K. Sharma, and B. S. Hsiao, "A simple approach to prepare carboxycellulose nanofibers from untreated biomass," *Biomacromolecules*, vol. 18, no. 8, pp. 2333–2342, 2017.

[37] R. Lafi, I. Montasser, and A. Hafiane, "Adsorption of Congo red dye from aqueous solutions by prepared activated carbon with oxygen-containing functional groups and its regeneration," *Adsorption Science & Technology*, vol. 37, no. 1-2, pp. 160–181, 2019.

[38] R. Ahmad and R. Kumar, "Adsorptive removal of Congo red dye from aqueous solution using bael shell carbon," *Applied Surface Science*, vol. 257, no. 5, pp. 1628–1633, 2010.

[39] C. Namasivayam and D. Kavitha, "Removal of Congo red from water by adsorption onto activated carbon prepared from coir pith, an agricultural solid waste," *Dyes and Pigments*, vol. 54, no. 1, pp. 47–58, 2002.

[40] D. Pathania, A. Sharma, and Z.-M. Siddiqi, "Removal of Congo red dye from aqueous system using Phoenix dactylifera seeds," *Journal of Molecular Liquids*, vol. 219, pp. 359–367, 2016.

[41] M. K. Purkait, A. Maiti, S. Dasgupta, and S. De, "Removal of Congo red using activated carbon and its regeneration," *Journal of Hazardous Materials*, vol. 145, no. 1-2, pp. 287–295, 2007.

[42] A. M. Aljeboree, A. N. Alshirifi, and A. F. Alkaim, "Kinetics and equilibrium study for the adsorption of textile dyes on coconut shell activated carbon," *Arabian Journal of Chemistry*, vol. 10, pp. S3381–S3393, 2017.

[43] J. Chukki, S. Abinandan, and S. Shanthakumar, "Chrysanthemum indicum microparticles on removal of hazardous Congo red dye using response surface methodology," *International Journal of Industrial Chemistry*, vol. 9, no. 4, pp. 305–316, 2018.

[44] P. Malik, "Dye removal from wastewater using activated carbon developed from sawdust: adsorption equilibrium and kinetics," *Journal of Hazardous Materials*, vol. 113, no. 1-3, pp. 81–88, 2004.

[45] E. D. Revellame, D. L. Fortela, W. Sharp, R. Hernandez, and M. E. Zappi, "Adsorption kinetic modeling using pseudo-first order and pseudo-second order rate laws: a review," *Cleaner Engineering and Technology*, vol. 1, article 100032, 2020.

[46] N. Malima, S. Owonubi, E. Lugwisha, and A. Mwakaboko, "Thermodynamic, isothermal and kinetic studies of heavy metals adsorption by chemically modified Tanzanian Malangali kaolin clay," *International journal of Environmental Science and Technology*, vol. 18, no. 10, pp. 3153–3168, 2021.

[47] X. Wang, C. Jiang, B. Hou, Y. Wang, C. Hao, and J. Wu, "Carbon composite lignin-based adsorbents for the adsorption of dyes," *Chemosphere*, vol. 206, pp. 587–596, 2018.

[48] N. Elhadiri, M. Benchanaa, and R. Chikri, "Adsorption thermodynamic and kinetic studies of methyl orange onto sugar scum powder as a low-cost inorganic adsorbent," *Journal of Chemistry*, vol. 2020, Article ID 9165874, 10 pages, 2020.

[49] G. Bayramoglu and M. Y. Arica, "Adsorption of Congo red dye by native amine and carboxyl modified biomass of Funalia trogii: isotherms, kinetics and thermodynamics mechanisms," *Korean Journal of Chemical Engineering*, vol. 35, no. 6, pp. 1303–1311, 2018.

[50] Y. El Maguana, N. Elhadiri, M. Benchanaa, and R. Chikri, "Activated carbon for dyes removal: modeling and understanding the adsorption process," *Journal of Chemistry*, vol. 2020, Article ID 2096834, 9 pages, 2020.

[51] S. Dawood and T. K. Sen, "Removal of anionic dye Congo red from aqueous solution by raw pine and acid-treated pine cone powder as adsorbent: equilibrium, thermodynamic, kinetics, mechanism and process design," *Water Research*, vol. 46, no. 6, pp. 1933–1946, 2012.

[52] P. Debnath and N. K. Mondal, "Effective removal of Congo red dye from aqueous solution using biosynthesized zinc oxide nanoparticles," *Environmental Nanotechnology, Monitoring & Management*, vol. 14, article 100320, 2020.

[53] F. Bessaha, N. Mahrez, K. Marouf-Khelifa, A. Çoruh, and A. Khelifa, "Removal of Congo red by thermally and chemically modified halloysite: equilibrium, FTIR spectroscopy, and mechanism studies," *International journal of Environmental Science and Technology*, vol. 16, no. 8, pp. 4253–4260, 2019.

[54] D. Pathania, S. Sharma, and P. Singh, "Removal of methylene blue by adsorption onto activated carbon developed from Ficus carica bast," *Arabian Journal of Chemistry*, vol. 10, pp. S1445–S1451, 2017.

[55] T. R. Mota, C. G. Kato, R. A. Peralta et al., "Decolourization of Congo red by Ganoderma lucidum laccase: evaluation of degradation products and toxicity," *Water, Air, & Soil Pollution*, vol. 226, no. 10, 2015.

[56] J. M. Jabar, Y. A. Odusote, K. A. Alabi, and I. B. Ahmed, "Kinetics and mechanisms of Congo-red dye removal from aqueous solution using activated Moringa oleifera seed coat as adsorbent," *Applied Water Science*, vol. 10, no. 6, 2020.

[57] V. B. Rao and S. R. M. Rao, "Adsorption studies on treatment of textile dyeing industrial effluent by flyash," *Chemical Engineering Journal*, vol. 116, pp. 77–84, 2006.

[58] T. A. Khan, S. Sharma, E. A. Khan, and A. A. Mukhlif, "Removal of Congo red and basic violet 1 by chir pine (Pinus roxburghii) sawdust, a saw mill waste: batch and column studies," *Toxicological & Environmental Chemistry*, vol. 96, no. 4, pp. 555–568, 2014.

[59] V. S. Mane and P. V. Babu, "Kinetic and equilibrium studies on the removal of Congo red from aqueous solution using Eucalyptus wood (Eucalyptus globulus) saw dust," *Journal of the Taiwan Institute of Chemical Engineers*, vol. 44, no. 1, pp. 81–88, 2013.

[60] S. Burca, C. Indolean, and A. Maicaneanu, "Isotherms study of Congo red biosorption equilibrium using FIR (*Abies nordmanniana*) sawdust biomass," *Revue Roumaine de Chimie*, vol. 62, pp. 381–389, 2017.

[61] J. N. Wekoye, W. C. Wanyonyi, P. T. Wangila, and M. K. Tonui, "Kinetic and equilibrium studies of Congo red dye adsorption on cabbage waste powder," *Environmental Chemistry and Ecotoxicology*, vol. 2, pp. 24–31, 2020.

[62] G. Sharma, T. S. AlGarni, P. S. Kumar et al., "Utilization of Ag_2O-Al_2O_3-ZrO_2 decorated onto rGO as adsorbent for the removal of Congo red from aqueous solution," *Environmental Research*, vol. 197, article 111179, 2021.